DOI: 10.4408/IJEGE.2020-01.S-12

ANALYSIS OF THE INCIDENT SEA - WAVES IN THE RODBREAK EXPERIMENT

Liliana V. PINHEIRO(*), João Alfredo SANTOS(**),
Jan Henk SPANS(***) & Conceição Juana E.M. FORTES(*)

(*)National Laboratory for Civil Engineering, Lisbon, Portugal.

(**)Instituto Superior de Engenharia de Lisboa, Instituto Politécnico de Lisboa and CENTEC - Centre for Marine Technology and Ocean Engineering, Lisbon, Portugal.

(***)Saxion University of Applied Sciences, Enschede, The Netherlands

Corresponding author: lpinheiro@lnec.pt

EXTENDED ABSTRACT

La campagna sperimentale RODBreak mira ad analizzare la risalita delle onde, la portata di tracimazione e il danno di una diga frangiflutti soggetta ad attacco ondoso obliquo. Un modello fisico di un tratto di tale struttura è stato realizzazto presso il laboratorio della Leibniz Universität di Hannover. Gli esperimenti nascono dalla volontà di voler approfondire l'analisi degli impatti del clima sulle strutture marittime, in generale, e sulle dighe frangiflutti nello specifico. L'innalzamento del livello del mare previsto, associato al verificarsi di mareggiate più frequenti ed intense, causerà un incremento di run-up, di portata tracimata e di danni sulle strutture esistenti, essendo state progettate considerando eventi estremi di intensità inferiore. Tuttavia, negli scenari di cambiamento climatico, non vi è una esaustiva conoscenza sulla risposta di tali strutture e sull'effettiva probabilità di fallimento. Il modello fisico della diga frangiflutti è stato testato in condizioni ondose estreme considerando differenti livelli di acqua, altezza significativa dell'onda (H_s), periodo di picco (T_p) e angolo dell'onda incidente. È stata contotta una sequenza di test per ciascun giorno lavorativo caratterizzata da un attacco ondoso con una specifica direzione dell'onda, una profondità dell'acqua e quattro valori di altezze d'onda incidenti (H_s = 0,100 m, 0,150 m, 0,175 m e 0,200 m e relativi periodi di picco T_p = 1,19 s, 1,45 s, 1,57 s e 1,68 s) e con stessa ripidità pari a 0,055. Gli stati di mare generati erano caratterizzati da uno spettro di tipo JONSWAP, con stesso directional spreading per tutte le frequenze generate di tipo cos2n. Per le onde lunghe e un livello di acqua di 0.60 m, sono stati considerati 5 angoli d'onda incidente (40 °, 55 °, 65°, 75 ° e 90 °). Poiché non erano previsti valori elevati di run-up, portate di tracimazione e danno lungo la sezione corrente della struttura per l'elevata obliquità degli attacchi ondosi, i test con livello 0.68 m in presenza di onde lunghe, sono stati eseguiti etstando solo 3 angoli di incidenza delle onde (40°, 55° e 65°). L'influenza del valore di directional spreading in presenza di onde corte è stata analizzata per livelli di acqua inferiori (0.60 m), con attacchi ondosi incidenti inclinati di 40° e 65°, e con directional spreading di 50°. La strumentazione utilizzata durante gli esperimenti ha consentito la misura delle caratteristiche ondose incidenti , la risalita dell'onda sulla struttura, le portate di tracimazione e il danno subito dallo strato di mantellata. La misura delle onde incidenti è stata eseguita attraverso l'utilizzo di 3 serie di sonde, ciscuna delle quali composta da 6 strumenti: la prima posta davanti al generatore di moto ondoso, la seconda e la terza, rispettivamente, davanti alla sezione di testata e centrale della struttura. Le sonde acustiche erano collegate ad un dispositivo di acquisizione HBM Catman che garantiva la sincronizzazione dei dati acquisiti, con una frequenza di campionamento di 300 Hz. Nel presente lavoro si riportano alcuni risultati derivanti dall'elaborazione dei dati di onde acquisiti in corrispondenza del generatore di onde. Sono state prese in considerazione tre procedure per la caratterizzazione dello stato del mare:

a) Per i dati raccolti sulla sonda centrale:

1. analisi nel dominio del tempo – caratterizzazione delle onde mediante metodo up-crossing e caclolo dell'altezza d'onda significativa e del periodo medio di zero-crossing;

2. spettro monodimensionale con definizione del periodo di picco e uso dei momenti spettrali per stimare l'altezza d'onda significativa e il periodo di energia medio;

b) Per i dati acquisiti dai 6 sensori:

3. stima dello spettro bidimensionale con il pacchetto DIWASP (Johnson, 2002; Pinheiro, 2019) utilizzando il metodo di massima verosimiglianza proposto da Isobe *et alii* (1984). Le analisi mirano alla definizione del più piccolo e del più grande stato di mare, coincidente con lo stato di mare incidente con un livello di acqua in vasca di 0.60 m. Nel presente lavoro si riportano i risultati ottenuti per gli stati di mare con angoli di incidenza massimo, minomo e intermedio, ovvero pari a 40°, 65° e 90°.

I risultati non mostrano differenze sostanziali nel calcolo delle altezze d'onda significative mediante l'utilizzo dei tre metodi, le quali non si discostano dai valori previsti. Per gli stati di mare meno energetici l'altezza d'onda significativa calcolata risulta essere maggiore di quella prevista , mentre il contrario accade per gli stati di mare energeticamente più elevati. I valori stimati del periodo di picco sono abbastanza vicini a quelli teorici e lo stesso accade per le direzioni d'onda stimate durante i test eseguiti in presenza di onde lunghe. Come previsto, i valori di ripidità delle onde sono fortemente influenzati dal periodo d'onda utilizzato per il calcolo. . Il valore della ripidità più prossimo al valore teorico di 0.055 è stato ottenuto utilizzando per il calcolo del periodo derivato dallo spettro unidimensionale.

ABSTRACT

The RODBreak experiment aimed at characterizing wave run-up, overtopping and damage in rubble-mound breakwaters with oblique wave incidence. a stretch of a rubble-mound breakwater was built in the wave basin of the Leibniz Universität Hannover. Under extreme wave conditions, with different incident wave angles (from 40° to 90°), a total of 49 tests were performed. Each test had different testing parameters, such as significant wave height (H_s), peak period (T_p) and wave direction. Also, for each test, different types of measurements were considered. This paper presents the results of processing some of the wave data measured in this experiment. After this chapter of introduction, there is a brief description of the scale model tests, focusing on the measurements made. It describes the techniques employed to analyze the measured wave data as well as the results of such processing. Some conclusions on the characteristics of the sea-waves generated in this experiment are also drawn.

Keywords: *sea-wave characterization, short-crested waves, directional spectrum, large scale experiments.*

INTRODUCTION

The RODBreak experiment aimed at characterizing wave run-up, overtopping and damage in rubble-mound breakwaters with oblique wave incidence.

The reason for these experiments was the huge impact that climate can have on maritime structures, particularly in rubble-mound breakwaters. In fact, the forecast sea level rise associated with more frequent and severe storms will have consequences either on the increase of wave runup, wave overtopping or on damage on existent structures, since they were not designed for those extreme values. However, for those climate change scenarios, little is known about the actual failure probability of such structures.

Within this framework, a stretch of a rubble-mound breakwater was built in the wave basin of the Leibniz Universität Hannover. Under extreme wave conditions, with different incident wave angles (from 40° to 90°), a total of 49 tests were performed. Each test had different testing parameters, such as significant wave height (H_s), peak period (T_p) and wave direction. Also, for each test, different types of measurements were considered.

This paper presents the results of processing some of the wave data measured in this experiment. After this chapter of introduction, there is a brief description of the scale model tests, focusing on the measurements made. Then the techniques employed to analyse the measured wave data are described as well as the results of such processing. The paper finishes with some conclusions on the characteristics of the sea-waves generated in this experiment.

SCALE - MODEL TESTS

A stretch of a rubble mound breakwater (head and part of the adjoining trunk, with a slope of 1 (V) : 2 (H)) was built in the wave basin of the Leibniz Universität Hannover.

The model axis made an angle of 70º to the tank wall opposite the wave maker. The total model length, measured along the crest axis, is 9.3 m and its width is 3.7 m, as can be seen in Figure 1. The armour layer of the breakwater head, as well as of the 2.5 m wide adjoining exposed strip, was made of two layers of 351 gf Antifer cubes. The remaining 5 m of the breakwater trunk had an armour layer made of rock (gravel) with a median weight of 315 gf. It was expected the porosity of the armour layer to be 37%. More details on the model can be found on the data storage report (Santos *et alii* 2019).

The wave tank is 40 m long, 25 m wide and 1 m deep. Along one of its longest sides it has a wave maker made of 72 paddles placed side by side. Each paddle is 0.40 m wide and 1.60 m high and works as a piston with a maximum excursion of ±0.60 m and a maximum velocity of 3.0 m/s and it can generate waves with a height of up to 0.47 m when the water depth is 1.0 m. The wave direction ranges from 0º to 75º with relation to the normal to the wave maker (or from 15º to 165º with relation to the x-axis shown in Fig. 1).

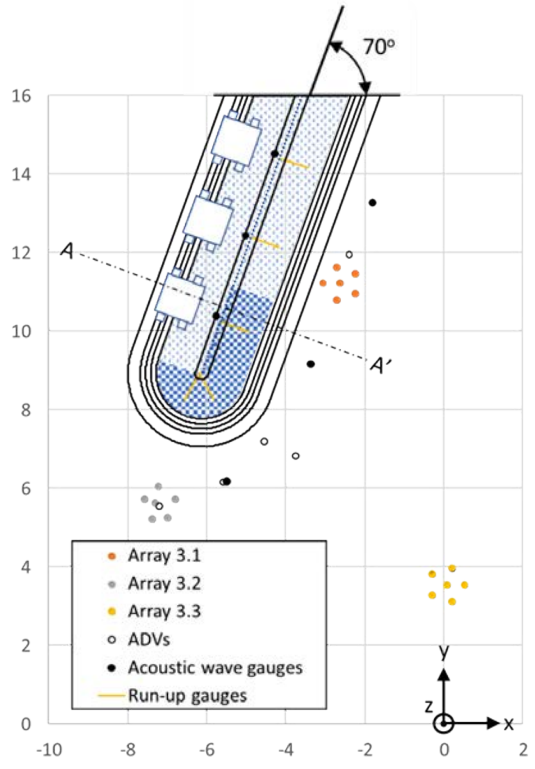

Fig. 1 - Plan view of breakwater model with equipment deployed at the tests.

Wave absorption in the wave tank is made by a passive and by an active system. Passive absorption is carried out by 8 metallic plates with different porosity placed within a strip 5 m wide along each side of the wave tank. Active absorption aims at cancelling re-reflection of waves at the wave maker. Each of the 72 paddles has sensors for free-surface elevation which are analysed at real time by the wave maker control software. It determines the paddle motion to ensure the required wave generation and the identified incident wave on the paddle.

One test sequence was carried out per working day and it consisted of one wave direction, one water depth and four incident sea-waves with growing significant wave height and the same wave steepness of 0.055. S_o, for the tested significant wave heights of H_s = 0.100 m, 0.150 m, 0.175 m and 0.200 m the corresponding peak periods were T_p = 1.19 s, 1.45 s, 1.57 s and 1.68 s. At the end of the test sequence the armour layer was rebuilt, i.e. the displaced armour elements were put back in their initial positions. All sea states generated in the tests were meant to have a JONSWAP frequency spectrum, the directional spreading function being the same for all generated frequencies and of cos2n-type.

For long-crested waves and a water depth of 0.60 m, 5 incidence wave angles (40°, 55°, 65°, 75° and 90°) were considered. Since no major run-up, overtopping or damage were expected along the structure for high incidence angles, in the test series with a water depth of 0.68 m and long-crested waves, the number of incidence angles was reduced to 3 (40°, 55° and 65°).

The influence of the directional spreading of short-crested waves was investigated for the lowest water depth (0.60 m) and the incidence angles of 40° and 65°, the directional spreading being 50°. Finally, for the incidence angle of 40° results were also obtained for the highest water depth (0.68 m) and short-crested waves with a directional spreading of 50°.

The equipment deployed in the experiment aimed at characterizing the incident sea-waves, the run-up, the overtopping events and the armour layer damage evolution. Figure 1 presents a plan view of the key instruments for those variables (apart from "armour layer damage"). The photo in Fig. 2 highlights the arrays of acoustic wave probes, which are the subject of this paper. The numbering of the instruments (x) increased from the breakwater root to the breakwater head.

Each array (3.1 to 3.3) was made of six acoustic wave gauges whose coordinates in the reference system of Fig. 1 are presented in Table 1. That reference system has its origin in the middle of rest position of the wavemaker width, between paddle 36 and 37. The acoustic wave gauges were connected to an HBM Catman data acquisition device which ensured the synchronization of the data collection at a 300 Hz sampling rate.

Array	*probe*	*x(m)*	*y(m)*
3.1	*3.1.1*	*-2.71*	*11.65*
	3.1.2	*-3.05*	*11.23*
	3.1.3	*-2.70*	*10.80*
	3.1.4	*-2.23*	*10.98*
	3.1.5	*-2.22*	*11.48*
	3.1.6	*-2.64*	*11.23*
3.2	*3.2.1*	*-7.55*	*5.75*
	3.2.2	*-7.39*	*5.24*
	3.2.3	*-6.99*	*5.26*
	3.2.4	*-6.80*	*5.75*
	3.2.5	*-7.23*	*6.06*
	3.2.6	*-7.29*	*5.63*
3.3	*3.3.1*	*-0.29*	*3.82*
	3.3.2	*-0.29*	*3.30*
	3.3.3	*0.21*	*3.14*
	3.3.4	*0.52*	*3.56*
	3.3.5	*0.22*	*3.99*
		0.08	*3.56*

Tab. 1 - Coordinates of the acoustic probes in the wave gauge arrays.

Fig. 2 - Breakwater model and acoustic wave arrays in the wave tank.

METHODOLOGIES FOR SEA-WAVE CHARACTERIZATION

The measurements from one array of acoustic wave gauges can be used to characterize the sea waves in the region where the array is deployed. The time series of the free-surface elevation measured by one acoustic wave gauge in the array can provide a characterization of the sea waves at the point where the wave gauge is deployed.

This suggests the use of two different approaches to characterize the sea-waves in the wave tank with the measurements made by one array of acoustic wave gauges.

The first one considers one wave probe alone, and makes use of the SAM package (Capitão, 2002). It encompassed the so-called:

- Analysis in the time domain with wave definition by consecutive zero up-crossing. This enabled the estimation of the significant wave height, H_s, by the average of the wave height in the third of the highest waves, as well as the mean zero crossing wave period, T_z;
- Analysis in the frequency domain, with the estimation of the one-dimensional spectrum and the computation of the spectral moments and of the moment-based significant wave height, $H_{m0} = (m_0)^{1/2}$, and mean energy period, $T_{m-1,0} = m_{-1}/m_0$.

The second one uses the whole array of acoustic wave probes to estimate the two-dimensional spectrum. This estimation was carried out with the DIWASP package (Johnson, 2002; Pinheiro, 2019**)** using the Extended Maximum Likelihood Method of Isobe *et alii* (1984). By integrating the two-dimensional spectrum in direction, one gets a one-dimensional frequency spectrum whose moments enable the estimation of the significant wave height and of the mean energy period, as explained above. Likewise, by integrating the two-dimensional spectrum in frequency, one gets a directional spectrum, from which the mean direction, θ_m, can be estimated as well as the directional spreading, σ_θ:

$$\sigma_\theta^2 = \int_{-\pi}^{\pi} \left[2\sin\left(\frac{\theta}{2}\right) \right]^2 D(\theta)\, d\theta \qquad (1)$$

θ being measured with relation to the average direction, θ_m.

Using the mean energy period, $T_{m-1,0}$, and the significant wave height, H_{m0}, the steepness of the sea state can be computed:

$$s_{0m-1,0} = H_{m0} / \left[g T_{m-1,0}^2 / 2\pi \right] \qquad (2)$$

It should be pointed out that, to speed up the data processing, it was decided to re-sample the data from the acoustic wave gauges. Instead of 300 Hz a smaller frequency of 100 Hz was considered.

RESULTS AND DISCUSSION

The objective of the analysis presented in this paper is to confirm that the sea-states generated in the experiment did match the requested characteristics in the test plan. So, this study focused on the wave array in front to the wave maker, array 3.3. For the analysis of one single acoustic wave gauge, the chosen one was probe 3.3.6, which lies in the centre of the array.

Table 2 presents the sea-state parameters estimated from those measurements. Only the smallest and the largest sea-state in the test series corresponding to one incident sea-state are presented. As to the incidence angle only results for the extreme and the middle angle, i.e. 40º, 65º and 90º, are presented. It must be pointed out that the mean direction angle presented in the table refers to the angle with the x-axis and is the direction from which the waves come. Hence, for the 40º incidence the wave direction is 300º, 275º for 65º and 250º for 90º. Only the smallest water depth (0.60 m) was considered.

The values in the table show that, as expected, there are no

Test					*Time domain*		*1-D wave spectrum*			*2-D wave spectrum*				
N.	H_s	T_p	θ_m	σ_θ	H_s	T_z	H_{m0}	T_p	$T_{m-1,0}$	H_{m0}	T_p	$T_{m-1,0}$	θ_m	σ_θ
13	0.100	1.19	300	0	0.108	0.97	0.101	1.19	1.08	0.104	1.20	0.98	300	4
16	0.200	1.68			0.195	1.27	0.191	1.68	1.47	0.197	1.71	1.28	303	4
17	0.100	1.19	275	0	0.111	0.95	0.105	1.16	1.06	0.109	1.20	0.97	276	3
20	0.200	1.68			0.190	1.27	0.186	1.65	1.48	0.193	1.69	1.28	276	3
21	0.100	1.19	250	0	0.118	0.96	0.110	1.19	1.09	0.110	1.20	0.96	251	4
25	0.200	1.68			0.187	1.22	0.181	1.65	1.47	0.194	1.71	1.28	251	4
35	0.100	1.19	300	50	0.117	0.92	0.113	1.15	1.04	0.113	1.19	0.96	309	46
38	0.200	1.68			0.187	1.23	0.184	1.66	1.47	0.193	1.71	1.28	298	43
40	0.100	1.19	275	50	0.118	0.93	0.111	1.18	1.05	0.114	1.20	0.95	291	46
43	0.200	1.68				1.24	0.192	1.66	1.47	0.195	1.69	1.28	288	44

Tab. 2 - Sea-wave parameters estimated from the measurements at the wave array in front of the wave maker (3.3).

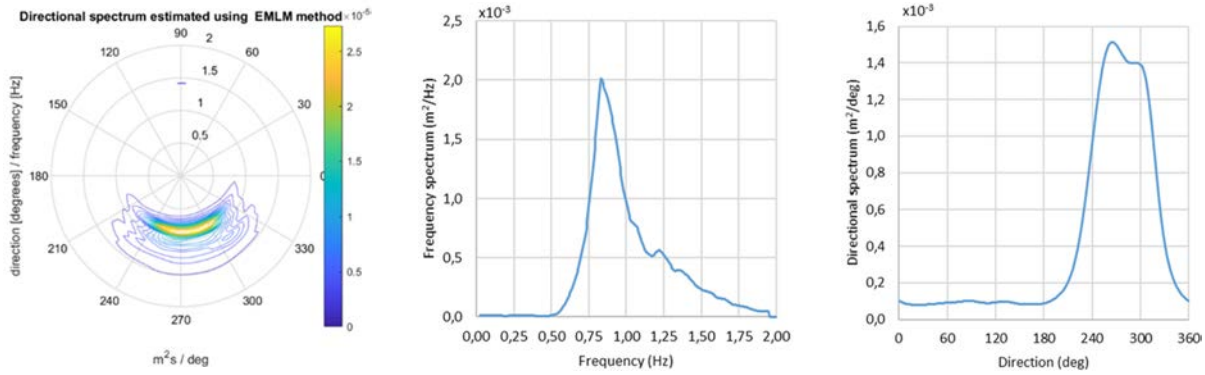

Fig. 3 - Sea wave characterization at test 40. Left: polar representation of two-dimensional spectrum; middle: frequency spectrum; right: directional spectrum.

major differences on the significant wave heights computed from the three approaches presented and they are not too far apart from the intended values. Small sea-states have a significant wave height larger (maximum of 18 mm in the time domain analysis) than the intended one and the opposite happens for the large sea-states (13 mm, in the time domain analysis). As to the peak period, it may be concluded that the values estimated from the measurements are quite close to the intended ones.

The wave directions estimated from the tests with long-crested waves are very close to the target values. There is a maximum difference of 3o for the wave direction which farthest from the normal to the wave maker. For the short-crested waves those differences are larger than for the long-crested waves and seem to be largest for the wave direction close to the normal to the wave maker. This can be a problem of the method used to estimate the two-dimensional spectrum.

In the right plot of Fig. 3 one may see that the directional spectrum does not have a clear decrease to zero away from the mean direction but rather a low energy level across those directions. This can be due to numerical problems in the estimation of the bi-dimensional spectrum.

Since the directional spreading of Eq. (1) is akin to the gyration radius of the area beneath the directional spectrum, such non-zero values may lead to directional spreading values much larger than the expected ones.

Hence, an automated procedure was established to define the interval containing the average direction to be considered in the evaluation of the integral in equation (1). For this one starts at $\theta = 0^o$ or $\theta = 360^o$ and moves towards θ_m computing the absolute value of the steepness of the directional spectrum between consecutive points as well as the average of those steepness values. When the local steepness equals ten times the average steepness, the search is finished for that side of the directional spectrum and one may move to the other end of the theta interval, where the procedure is repeated.

Figure 4 illustrates such a procedure for the directional spectrum of test 40. In addition to the directional spectrum, the figure presents the curve for the ratio between the local steepness to the average of consecutive steepness values. In this case starting from $\theta = 0^o$, one finds the lower end of the integration integral at approximately $\theta = 210^o$. When starting from $\theta = 360^o$ the steepness ratio never reaches the level ten, but this is no problem since the directional spectrum is clearly rising at that end of the interval.

The directional spreading in Table 2 were obtained with this procedure. The table shows that for the long-crested sea-states the directional spreading values are around 4^o. For the short-crested sea-states that value ranges from 43^o to 46^o, which is substantially larger than the values for the long-crested sea-states and close to the intended value of 50^o.

Table 3 presents the sea-state steepness in front of the wave maker evaluated with the significant wave height and average period of the sea-state estimated from both point measurements and array measurements. The values in the "Time domain" row were computed with the deep-water wave length corresponding

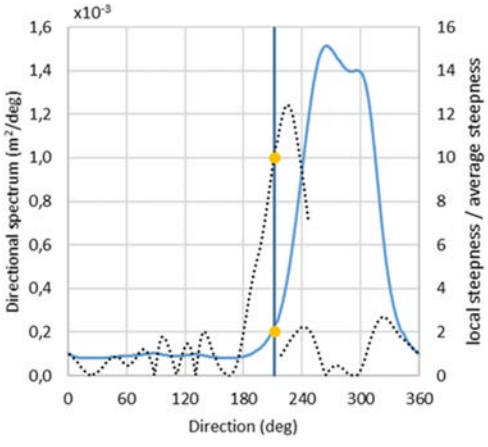

Fig. 4 - Determination of the limits of integration of the directional spectrum for Test040.

Test	*T013*	*T016*	*T017*	*T020*	*T021*	*T025*	*T035*	*T038*	*T040*	*T043*
Time domain	*0.073*	*0.078*	*0.078*	*0.076*	*0.082*	*0.081*	*0.089*	*0.079*	*0.087*	*0.081*
1-D spectrum	*0.056*	*0.056*	*0.059*	*0.054*	*0.059*	*0.054*	*0.067*	*0.054*	*0.065*	*0.057*
1-D spectrum (s_0m01)	*0.063*	*0.068*	*0.068*	*0.065*	*0.069*	*0.066*	*0.076*	*0.065*	*0.073*	*0.068*
1-D spectrum (s_0m)	*0.056*	*0.052*	*0.060*	*0.052*	*0.060*	*0.052*	*0.066*	*0.052*	*0.062*	*0.054*
2-D spectrum	*0.070*	*0.077*	*0.074*	*0.075*	*0.076*	*0.076*	*0.079*	*0.075*	*0.080*	*0.077*

Tab. 3 - Steepness of the sea-state in front of the wave maker

to the mean zero-crossing wave period, whereas for the values in "1-D spectrum ($s_{0,m01}$)" and the "1-D spectrum (s_{0m})" rows the same wave length was obtained, respectively, from the average spectral period ($T_{m01}=m_0/m_1$) and the mean zero-crossing period ($T_m=T_p/1.1$), which is a classical result for the JONSWAP spectrum.

It must be pointed out that the peak period for each test was obtained using this result and the corresponding significant wave height was the result of forcing the sea-state steepness to be equal to 0.055 and the deep-water wavelength used in the computations corresponded to this mean zero-crossing period. The values in the remaining two rows were obtained with the mean energy period.

The table shows that the steepness values from the two-dimensional spectrum, whose deep-water wavelengths are obtained with the mean energy period, are clearly above the requested value.

The same happens with the values from the one-dimensional spectrum with the average spectral period ($s_{0,m01}$) and from the time domain values.

The steepness values computed from the one-dimensional spectrum and the deep-water wavelengths from $T_m=T_p/1.1$ are closer to the 0.055 value.

This is no surprise since the peak periods of the experiment were established with that relation and forcing s_{0m} = 0.055. What is probably more interesting in Table 3 is the result obtained with the energy period from the one-dimensional spectrum. The steepness values are like the previous ones and close to the 0.055 value.

CONCLUSIONS

Some of the results from processing the wave data collected at the array of acoustic wave gauges deployed in front of the wave maker in the RODBreak experiment were presented in this paper. Three procedures were considered for the sea-state characterization: time domain analysis and one-dimensional spectrum for the data collected at the central probe of the array and two-dimensional spectrum for the whole array. They show that there are no major differences on the significant wave heights computed from the three approaches presented and they are not too far apart from the intended values. Small sea-states have a significant wave height larger than the intended one and the opposite happens for the large sea-states. The estimated peak period values are quite close to the intended ones and the same happens for the wave directions estimated from the tests with long-crested waves.

As expected, the values of sea-state steepness depend strongly of the period used in their computation. The values obtained for the energy period from the one-dimensional spectrum are the closest to the 0.055 intended value.

ACKNOWLEDGMENTS

This project has received funding from the European Union's Horizon 2020 research and innovation programme under grant agreement No 654110, HYDRALAB+.

The project To-SEAlert - Wave overtopping and flooding in coastal and port areas: Tools for an early warning, emergency planning and risk management system, Ref. PTDC/EAM-OCE/31207/2017 is also acknowledged.

REFERENCES

Booij N., Ris R.C. & Holthuijsen L. H. (1999) - *A third-generation wave model for coastal regions. 1. Model Description and validation* - J. Geophys. Res, **104**: 7649 - 7666.

Capitão R., (2001) - *Numerical and Physical Stochastic Modelling of Sea Waves* (in Portuguese). PhD thesis Universidade Técnica de Lisboa, Portugal.

Isobe M., Kondo K., Horikawa K. (1984) - *Extension of MLM for estimating directional wave spectrum.* Proc. Symp. on Description and Modeling of Directional Seas, Paper No. **A - 6**: 15 pp.

Johnson D. (2002) - *DIWASP, A directional wave spectra toolbox for MATLAB®: User Manual*. Research Report WP-1601-DJ, Centre for Water Research, University of Western Australia.

Pinheiro L.V. (2019) - *MATLAB script with DIWASP plugin,* LNEC, Lisbon.

Santos J.A., Lemos R., Weimper J., Gronz O., Hofland B., Sande J., Peña E., Reis M.T., Fortes C.J., Figuero A., Bornschein A., Kerpen N., Pedro F., Coimbra M., Körner M., van den Bos J., Dost B., Carvalho R., Alvarellos A., Pohl R. (2019) - *Data Storage Report. RODBreak - Wave run-up, overtopping and damage in rubble-mound breakwaters under oblique extreme wave conditions due to climate change scenarios.* https://doi.org/10.5281/zenodo.3355657.

Received September 2019 - Accepted January 2020